

# A combined first and second order traffic network model

Jennifer Kötz\*, Oliver Kolb\*, Simone Göttlich\*

January 27, 2023

## Abstract

Second order macroscopic traffic flow models are well-known to be able to reproduce the so-called capacity drop effect, i.e., the phenomenon that the outflow of a congested region is substantially lower than the maximum achievable flow in this particular area. Within this work, we propose a first order network model that is solely modified at the intersection points so that the capacity drop is captured. Theoretical investigations motivate the new choice of coupling conditions and illustrate the difference to purely first and second order network models. A numerical example considering the optimal control of an on-ramp merging into a main road highlights that the combined model generates similar results as a second order model but at significantly lower computational costs.

**AMS subject classifications:** 90B20, 35L65

**Keywords:** traffic flow, coupling conditions, capacity drop

## 1 Introduction

Starting with the pioneering works on the Lighthill-Whitham-Richards (LWR) model [18, 21], traffic flow models based on scalar conservation laws, i.e., macroscopic traffic models, have received considerable attention in the academic literature over the past decades. Macroscopic models are mainly distinguished in first order models, which consist of a scalar conservation law for the traffic density, and second order models, using a system of two conservation or balance laws with an additional equation for the mean traffic speed. The main drawback of the LWR model is the direct link of the velocity and flux to the traffic density, which does not allow for a correct description of traffic instabilities. Second order models have been developed aiming at correcting these deficiencies, see [5]. Aw and Rascle [1] introduced a second order traffic model which is capable to capture traffic instabilities and additionally overcame the drawbacks of earlier developed second order models. Greenberg [10] extended their model with a relaxation term towards a preferred velocity. Since then, the extension to traffic flow on road networks has been investigated intensively, see for example [2, 3, 8, 9, 11, 13, 14, 16, 20]. The crucial point in a network setting is the definition of suitable coupling conditions, i.e. conservation of mass and possibly momentum in the case of second order models.

So-called multiscale approaches couple traffic flow models of different scales at fixed interfaces and combine them via suitable coupling conditions at this interface. Multiscale

---

<sup>1</sup>University of Mannheim, Department of Mathematics, 68131 Mannheim, Germany (jkoetz@mail.uni-mannheim.de, {kolb,goettlich}@uni-mannheim.de).

approaches involving the LWR model and the model of Aw and Rascle (AR) that couple microscopic and macroscopic models have been investigated in [6] and [19], respectively. A further approach are so-called phase transition models, combining two macroscopic approaches based on the traffic states of free flow and the congested phase. Phase transition models are obtained by the coupling of two different models at a free boundary, e.g., by a threshold speed, where the transition between the two phases occurs. Above the threshold speed, the traffic is categorized as free flow, otherwise as congested flow. Typically, a first order model is used for the free flow phase, while the congested zone is portrayed by a second order model. The main difficulty for such kind of models is to introduce a transition dynamics from free flow to congested flow and vice versa. Similar to several (full) second order models, phase transition models are known to be able to reproduce the capacity drop effect, see [4, 7].

In contrast to the mentioned approaches, we completely stick to a first order model to describe the dynamics on the roads. To mirror the capacity drop effect, we put special emphasis on the intersections of the network, where the velocities are incorporated to describe the dynamics. The main advantage of this approach in comparison to the phase transition models is the simplicity, since we consider a first order macroscopic model on the roads, whereas we merely apply adapted coupling conditions of a second order macroscopic model at the junctions. This combination then allows to model the capacity drop effect. A similar approach has been considered in [12], where the LWR model was coupled to a kinetic model at the junctions. Comparable to [12], our setup is also able to cover the capacity drop phenomenon. A further advantage of the combined approach can be seen when investigating optimal control strategies for ramp metering and variable speed limits [8, 9].

The paper is organized as follows: In Section 2, we briefly recall the LWR and AR network model for traffic flows and introduce the combined model. We define the respective demand and supply functions, which determine the flux at the junction and explain the coupling conditions for different types of junctions. Section 3 is devoted to a theoretical discussion of the proposed combined model, where we also provide comparisons to the LWR and AR model. A discussion on Riemann problems for the combined model is given in Sections 3.2 and 3.3. The paper concludes with numerical results for an optimal control problem including ramp metering in Section 4.

## 2 Models for traffic flow on road networks

We consider a directed graph  $G = (V, E)$  with a finite number of roads  $e \in E$  and junctions  $j \in V$ . The roads  $e$  are modeled by intervals  $(a_e, b_e)$  with possibly infinite lengths. Vehicles are treated as a continuum with density  $\rho$  and velocity  $v$ . We shortly introduce two well-known first and second order macroscopic approaches for traffic flow. Then, we establish a new modeling approach, which combines first and second order traffic information at junction points leading to new coupling conditions.

### 2.1 The LWR model

Given an initial state  $\rho_e(x, 0)$  on each road  $e$ , the dynamics of the LWR traffic flow model [18, 21] is given by

$$\partial_t \rho_e(x, t) + \partial_x f_e(\rho_e(x, t)) = 0 \quad \forall e \in E, x \in (a_e, b_e), t \in (0, T)$$

with

$$f_e(\rho) = \rho \cdot V_e(\rho) = \rho v_e^{\max} \left(1 - \frac{\rho}{\rho_e^{\max}}\right).$$

Traffic flow  $f_e$  and velocity  $V_e$  are directly coupled to the traffic density  $\rho_e$  and  $\rho_e^{\max}, v_e^{\max}$  denote the maximal density or velocity, respectively. For the description of coupling and boundary conditions, we introduce the widely used demand and supply functions [8]

$$D_e^{\text{LWR}}(\rho) = \begin{cases} f_e(\rho) & \text{if } \rho \leq \frac{\rho_e^{\max}}{2}, \\ f_e^{\max} & \text{otherwise,} \end{cases}$$

$$S_e^{\text{LWR}}(\rho) = \begin{cases} f_e^{\max} & \text{if } \rho \leq \frac{\rho_e^{\max}}{2}, \\ f_e(\rho) & \text{otherwise,} \end{cases}$$

where  $f_e^{\max} = f_e\left(\frac{\rho_e^{\max}}{2}\right)$  is the maximum flux on road  $e$ .

## 2.2 The AR model

In the second order model by Aw and Rascle [1], the traffic density  $\rho_e = \rho_e(x, t)$  and velocity  $v_e = v_e(x, t)$  are not directly coupled, but evolve according to a system of conservation/balance laws. Given initial densities and velocities, the traffic dynamics are governed by the equations

$$\begin{aligned} \partial_t \rho_e + \partial_x(\rho_e v_e) &= 0, \\ \partial_t(\rho_e w_e) + \partial_x(\rho_e v_e w_e) &= -\rho_e \frac{v_e - V_e(\rho)}{\delta}, \\ w_e &= v_e + p_e(\rho_e), \end{aligned}$$

where we consider a relaxation term on the right-hand side of the second equation according to [10]. The first equation describes the conservation of mass and the second equation includes the evolution of the vehicle speed. The relaxation term on the right-hand side includes that drivers tend to adopt the preferential speed  $V_e(\rho)$ . The pressure function  $p_e(\rho)$  represents an anticipation factor, which takes into account the reaction of drivers to the traffic in front of them [7]. Introducing the variable  $y_e = \rho_e w_e$ , the above system can be written in conservative form:

$$\partial_t \begin{pmatrix} \rho_e \\ y_e \end{pmatrix} + \partial_x \begin{pmatrix} y_e - \rho_e p_e(\rho_e) \\ (y_e - \rho_e p_e(\rho_e)) \frac{y_e}{\rho_e} \end{pmatrix} = \begin{pmatrix} 0 \\ -\frac{(y_e - \rho_e p_e(\rho_e)) - \rho_e V_e(\rho)}{\delta} \end{pmatrix}.$$

Following [9], we consider a specific preferential speed function  $V_e(\rho)$  (according to the LWR flux),

$$V_e(\rho) = v_e^{\max} \left(1 - \frac{\rho_e}{\rho_e^{\max}}\right),$$

and the pressure function

$$p_e(\rho) = \frac{v_e^{\text{ref}}}{\gamma_e} \left(\frac{\rho_e}{\rho_e^{\max}}\right)^{\gamma_e}. \quad (1)$$

Here,  $v_e^{\text{ref}}$  denotes the reference velocity. The pressure function satisfies  $p'_e(\rho) > 0$  and  $\rho p''_e(\rho) + 2p'_e(\rho) > 0$  for all  $\rho$ . The first property ensures that the pressure function can be inverted and the second the existence of a point  $\sigma_e(c)$  that maximizes the flux  $\rho v$  for a fixed  $w = c$ . The inverse function of the pressure function is given by

$$p_e^{-1}(\bar{p}) = \rho_e^{\max} \left( \frac{\bar{p}\gamma_e}{v_e^{\text{ref}}} \right)^{\frac{1}{\gamma_e}},$$

and  $\sigma_e$  can also be computed explicitly,

$$\sigma_e(c) = \underset{\rho, w=c}{\operatorname{argmax}} \rho v = \underset{\rho, w=c}{\operatorname{argmax}} \rho(w - p(\rho)) = \rho_e^{\max} \left( \frac{c\gamma_e}{v_e^{\text{ref}}(1 + \gamma_e)} \right)^{\frac{1}{\gamma_e}}.$$

As stated in [9], the following demand and supply functions are considered for the AR model:

$$D_e^{\text{AR}}(\rho, c) = \begin{cases} (c - p_e(\rho))\rho & \text{if } \rho \leq \sigma_e(c), \\ (c - p_e(\sigma_e(c)))\sigma_e(c) & \text{otherwise,} \end{cases}$$

$$S_e^{\text{AR}}(\rho, c) = \begin{cases} (c - p_e(\sigma_e(c)))\sigma_e(c) & \text{if } \rho \leq \sigma_e(c), \\ (c - p_e(\rho))\rho & \text{otherwise.} \end{cases}$$

### 2.3 The combined model

In the macroscopic first order LWR model, velocity and flux are directly linked to the traffic density. Although the LWR model can predict some traffic situations rather well, the model exhibits various deficits [5]. In general, the model cannot portray traffic instabilities, which include growing traffic waves and so-called capacity drops. A recent study of the AR model on networks [9] shows that the second order AR model is able to portray the capacity drop, but comes at increased computational costs. Our idea is now to customize the coupling conditions of the LWR model in such a way that a capacity drop similar to the AR model can be achieved. We denote the new model as augmented LWR model, or shortly ALWR. For the coupling conditions proposed here, we introduce a quite useful partition of the phase plane, which we will explain in detail in Section 3.2.

Initially, we define the following demand and supply functions for the formulation of coupling and boundary conditions at a junction  $j$ :

$$D_e^j(\rho) = D_e^{\text{LWR}}(\rho) \tag{2}$$

$$S_e^j(\rho, \tilde{\rho}, c) = \begin{cases} S_e^{\text{LWR}}(\rho) & \text{if } 0 \leq f_e^{\text{sum}} \leq f_e^{\text{max}} \\ \min\{S_e^{\text{LWR}}(\rho), S_{\text{weighted}}(\rho, \tilde{\rho}, c)\} & \text{if } f_e^{\text{max}} \leq f_e^{\text{sum}} \leq (1 + \epsilon)f_e^{\text{max}} \\ \min\{S_e^{\text{LWR}}(\rho), S_e^{\text{AR}}(\tilde{\rho}, c)\} & \text{otherwise} \end{cases} \tag{3}$$

where

$$S_{\text{weighted}}(\rho, \tilde{\rho}, c) = S_e^{\text{AR}}(\tilde{\rho}, c) + (S_e^{\text{LWR}}(\rho) - S_e^{\text{AR}}(\tilde{\rho}, c)) \left( 1 - \frac{f_e^{\text{sum}} - f_e^{\text{max}}}{\epsilon f_e^{\text{max}}} \right) \tag{4}$$

with a smoothing parameter  $\epsilon$ . According to the AR model, the value of  $c$  corresponds to a given level of  $w = v + p(\rho)$ . Further,  $\tilde{\rho} = \tilde{\rho}(c, v)$  is the density that would arise from the velocity  $v$  behind the junction and the  $w$ -value  $c$  at the junction  $j$ , which is also used in the AR model, see [9]. The value

$f_e^{\text{sum}}$  indicates the cumulated desired inflow into road  $e$ , i.e., the sum of the demands of the roads and on-ramps that enter road  $e$ .

To determine the demand of an incoming road at a junction, the demand function of the LWR model is applied. In case that the cumulated desired inflow at a junction into road  $e$ , denoted by  $f_e^{\text{sum}}$ , does not exceed the maximum flow/capacity  $f_e^{\text{max}}$  of the outgoing road  $e$ , we also apply the supply function of the LWR model. In contrast, to evaluate the supply at a junction when the desired inflow exceeds the maximum capacity of the road, the minimum of the LWR supply for  $\rho$  and of the AR supply for  $\tilde{\rho}$  (see again [9]) is used. The transition phase with parameter  $\epsilon$  has been introduced to avoid a discontinuity in the proposed supply function at  $f_e^{\text{sum}} = f_e^{\text{max}}$ . Next, the introduced demand and supply functions are used to model boundary and coupling conditions for specific types of junctions that are depicted in Figure 1. Note that other intersection types are omitted since they do not impact on the capacity drop effect.

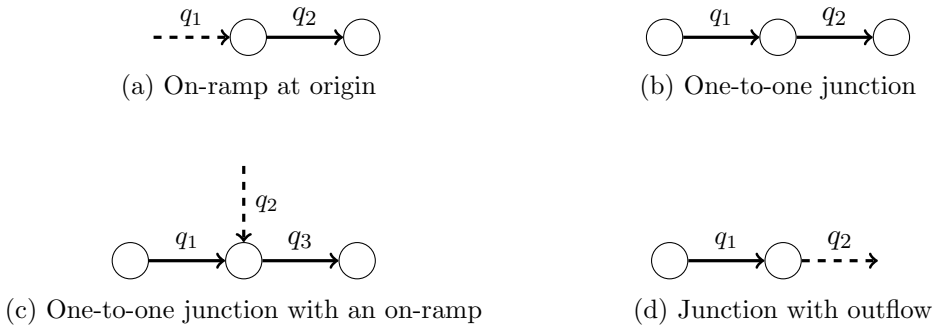


Figure 1: Types of junctions in the traffic network.

### One-to-one junction

We begin with a one-to-one junction and denote the ingoing road with index 1 and the outgoing road with index 2. Given the states  $\rho_1$  and  $\rho_2$  at the adjacent boundaries of roads 1 and 2, the flux  $q$  at one-to-one junctions is given by the minimum of the demand  $D_1^j$  evaluated at  $\rho_1$  and the supply  $S_2^j$  with  $\rho = \rho_2$ ,  $\tilde{\rho} = \tilde{\rho}_2 = \tilde{\rho}(w_1, V_2(\rho_2))$  and  $c = w_1$ , where  $w_1 = V_1(\rho_1) + p_1(\rho_1)$ . Note that  $\tilde{\rho}_2$  is determined in line with the AR model based on the equilibrium velocities  $v_i = V_i(\rho_i)$ . We get

$$q = q_1 = q_2 = \min\{D_1^j(\rho_1), S_2^j(\rho_2, \tilde{\rho}_2, w_1)\}$$

with

$$\tilde{\rho}_2 = p_2^{-1}(\max\{w_1 - v_2, 0\}) \quad w_1 = V_1(\rho_1) + p_1(\rho_1), \quad v_2 = V_2(\rho_2).$$

### One-to-one junction with an on-ramp

Next, we consider a one-to-one junction with an additional on-ramp. Here, we denote the ingoing road with index 1, the on-ramp with index 2 and the outgoing road with index 3. For roads 1 and 3 we assume (boundary) states  $\rho_1$  and  $\rho_3$ , and queue length  $l_2$  at the on-ramp. As in [8], we apply the demand function

$$D_2^j(l_2, t) = u_2(t) \begin{cases} f_2^{\text{max}} & \text{if } l_2 > 0, \\ \min\{f_2^{\text{in}}(t), f_2^{\text{max}}\} & \text{otherwise} \end{cases}$$

for the on-ramp, where  $u_2(t) \in [0, 1]$  is a time-dependent metering rate,  $f_2^{\text{in}}(t)$  the desired inflow of cars arriving at the on-ramp and  $f_2^{\text{max}}$  the maximum flux allowed from the on-ramp. To get a unique

solution, we assign priority parameters  $P$  and  $1 - P$  to road 1 and the on-ramp, respectively, and use

$$\begin{aligned} q_1 &= \min\{D_1^j(\rho_1), \max\{PS_3^j(\rho_3, \tilde{\rho}_3, w_1), S_3^j(\rho_3, \tilde{\rho}_3, w_1) - D_2^j(l_2, t)\}\}, \\ q_2 &= \min\{D_2^j(l_2, t), \max\{(1 - P)S_3^j(\rho_3, \tilde{\rho}_3, w_1), S_3^j(\rho_3, \tilde{\rho}_3, w_1) - D_1^j(\rho_1)\}\}, \\ q_3 &= q_1 + q_2 \end{aligned}$$

with

$$\tilde{\rho}_3 = p_3^{-1}(\max\{w_1 - v_3, 0\}) \quad w_1 = V_1(\rho_1) + p_1(\rho_1) \quad v_3 = V_3(\rho_3).$$

In comparison to the on-ramp model in [8], only the supply function  $S_3^j$  of the outgoing road has been adapted to the augmented model. Based on the computed fluxes, the evolution of the queue at the on-ramp is given by

$$\frac{dl_2(t)}{dt} = f_2^{\text{in}}(t) - q_2,$$

where we usually start with empty queues, i.e.,  $l_2(0) = 0$ .

### On-ramp at origin

We consider an on-ramp at a junction with only one outgoing road, where we denote the on-ramp by index 1 and the outgoing road with index 2. As above, the demand function of the on-ramp is given by

$$D_1^j(l_1, t) = u_1(t) \begin{cases} f_1^{\text{max}} & \text{if } l_1 > 0, \\ \min\{f_1^{\text{in}}(t), f_1^{\text{max}}\} & \text{otherwise,} \end{cases}$$

with metering rate  $u_1(t) \in [0, 1]$ , desired inflow  $f_1^{\text{in}}(t)$  and maximum flux  $f_1^{\text{max}}$ . To apply the augmented supply function, a value for  $w$  at the junction is necessary. Here, we follow the approach of [9] for the corresponding setting within the AR model, i.e.,

$$w_1 = V_2(\rho_-) + p_2(\rho_-) \tag{5}$$

with

$$\rho_- = \frac{\rho_2^{\text{max}}}{2} - \sqrt{\max\left\{0, \frac{(\rho_2^{\text{max}})^2}{4} - \frac{\rho_2^{\text{max}} D_1^j(l_1, t)}{v_2^{\text{max}}(t)}\right\}}.$$

Then, the flux going onto the road is given by

$$q_2 = \min\{D_1^j(l_1, t), S_2^j(\rho_2, \tilde{\rho}_2, w_1)\}$$

with

$$\tilde{\rho}_2 = p^{-1}(\max\{w_1 - v_2\}) \quad v_2 = V_2(\rho_2).$$

and  $w_1$  from (5). The evolution of the queue at the origin is given by

$$\frac{dl_1(t)}{dt} = f_1^{\text{in}}(t) - q_2.$$

### Junction with outflow

At a junction with only one ingoing road (denoted by index 1), we consider absorbing boundary conditions up to a given maximum flow rate  $f_1^{\text{out}}(t)$ ,

$$q_1 = \min\{D_1^j(\rho_1), f_1^{\text{out}}(t)\}.$$

### 3 Analysis of the ALWR model

This section focuses on the theoretical discussion of the supply function in the combined model. To show that the ALWR model is able to cover the capacity drop phenomenon, we study a one-to-one junction with on-ramp. In our discussion, the incoming and outgoing road possess identical parameters. The main difference to the network approach presented in [8] is the modelling of the supply at the junction of the network, where we impose second-order-like conditions in the supply function, cf. Section 2. For the particular setting, solutions of Riemann problems are discussed and phase space trajectories are compared to the LWR model.

#### 3.1 The augmented supply function

To analyze the differences between the LWR and the ALWR model, we start with an analysis of the term  $S_e^{AR}(\tilde{\rho}, c)$  in the augmented supply function  $S_e^j$ . Note that the ALWR model is identical to the LWR model in case of one-to-one junctions. Therefore, the analysis is focused on the situation of a one-to-one junction with on-ramp and Riemann initial data as depicted in Figure 2. Here, the incoming road is denoted with index  $l$  and the outgoing road with index  $r$ . Initial data is then given by

$$\rho(x, 0) = \begin{cases} \rho_l & \text{for } x \in (-\infty, 0), \\ \rho_r & \text{for } x \in (0, +\infty), \end{cases}$$

and a fixed demand  $D_{\text{onramp}}^j(l_{\text{onramp}}, t) = D_{\text{onramp}}^j(l_{\text{onramp}})$  from the on-ramp. Further, the case  $f_r^{\text{sum}} = D_l(\rho_l) + D_{\text{onramp}}^j(l_{\text{onramp}}) > (1 + \epsilon)f_r(\frac{\rho_r^{\text{max}}}{2})$  is considered.

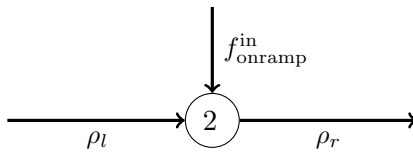


Figure 2: On-ramp setting.

Since the dynamics of vehicles on roads is described by the LWR model, the term  $S_r^{AR}(\tilde{\rho}, c)$  reduces to  $S^{AR}(\tilde{\rho}, w_l)$  with  $w_l = w(\rho_l)$  and reads

$$S^{AR}(\tilde{\rho}, w_l) = \begin{cases} (w_l - p(\sigma_l))\sigma_l & \text{if } \tilde{\rho} \leq \sigma_l, \\ (w_l - p(\tilde{\rho}))\tilde{\rho} & \text{otherwise,} \end{cases}$$

where  $\sigma_l = \sigma(\rho_l)$  is the sonic point given by

$$\sigma_l = \rho^{\max} \left( \frac{w_l \gamma}{v^{\text{ref}}(1 + \gamma)} \right)^{\frac{1}{\gamma}}.$$

Due to the dependence on  $w_l = w(\rho_l)$  (see Figure 3 for a plot of the function with  $\gamma = 2$ ), the value  $\rho_l$  scales the supply function up and down and also determines the position of the sonic point  $\sigma_l$ . The value  $\tilde{\rho}$ , which is used to evaluate the supply, is dependent on the combination of  $\rho_l$  and  $\rho_r$ . In particular,  $\tilde{\rho}$  decides which branch of the supply function  $S^{AR}$  is evaluated.

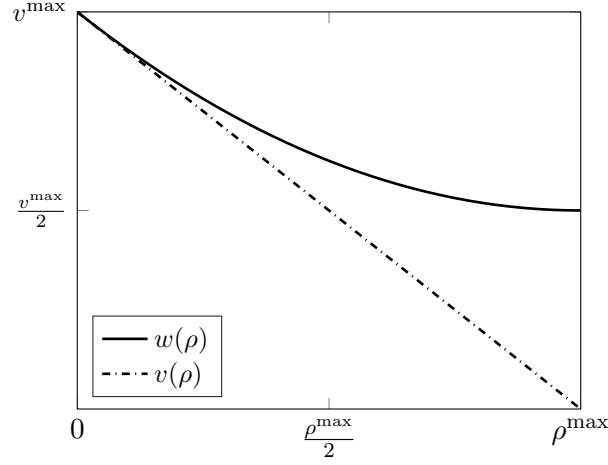


Figure 3:  $w$ -values and velocities.

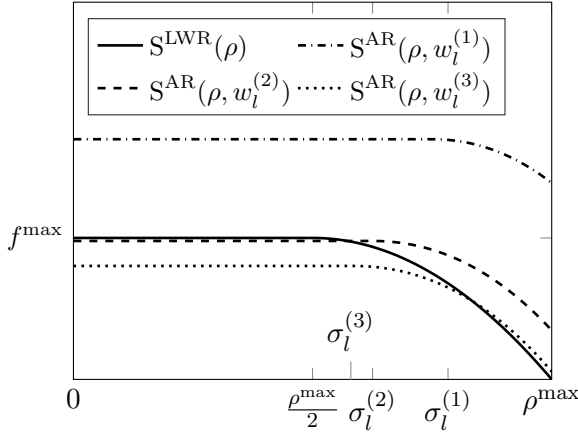


Figure 4: AR- and LWR-supply.

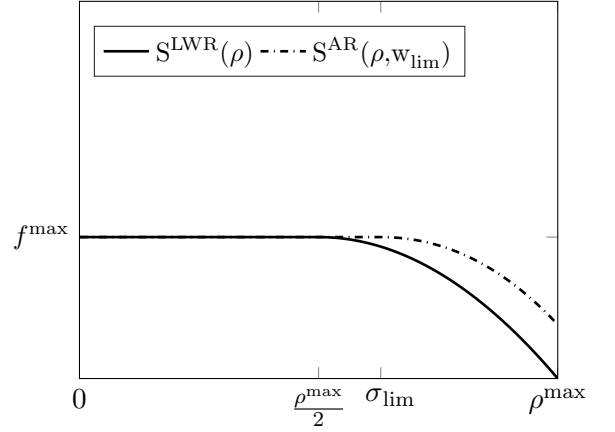


Figure 5: Limiting case  $w_{\text{lim}}$ .

Figure 4 shows the structure of the supply function in the AR model ( $\gamma = 2$ ) for different values  $w^{(1)}$  -  $w^{(3)}$  and the supply function of the LWR model. Different possibilities for the relation of the supply functions  $S^{\text{AR}}(\rho, w_l)$  and  $S^{\text{LWR}}(\rho)$  exist, see Figure 4:

1. the AR-supply  $S^{\text{AR}}(\rho, w_l^{(1)})$  exceeds the LWR-supply for all values of  $\rho$ ,
2. the AR-supply  $S^{\text{AR}}(\rho, w_l^{(2)})$  for small  $\rho$  is below the LWR-supply, but exceeds it onwards from some value  $\rho_r \leq \sigma(\rho_l)$ ,
3. the AR-supply  $S^{\text{AR}}(\rho, w_l^{(3)})$  for  $\rho \leq \sigma(\rho_l)$  is below the LWR-supply and the AR-supply exceeds the LWR-supply onwards from some value  $\rho \geq \sigma(\rho_l)$ ,
4. the AR-supply is equal to the LWR-supply for all  $\rho \leq \frac{\rho^{\text{max}}}{2}$  and exceeds it for  $\rho \geq \frac{\rho^{\text{max}}}{2}$  (limiting case, shown in Figure 5).

Note that we get the same possibilities also for  $\gamma > 1$ . In general, the  $w$ -value of the limiting case



is

$$w_{\text{lim}} = \left( \frac{f\left(\frac{\rho^{\text{max}}}{2}\right)}{\rho^{\text{max}} \left(\frac{\gamma}{v^{\text{ref}}(1+\gamma)}\right)^{\frac{1}{\gamma}} \frac{\gamma}{1+\gamma}} \right)^{\frac{\gamma}{\gamma+1}}. \quad (6)$$

Whether there is a restriction in the supply of the ALWR model in comparison to the LWR model depends on the value of  $w_l$ , which scales the supply function, and on the combination of the values  $\rho_l$  and  $\rho_r$ , which determine the value of  $\tilde{\rho}$ . Small  $w_l$  and  $\tilde{\rho}$ ,  $\rho_r$  lead to a restriction in comparison to the LWR-supply, while small  $w_l$  and large  $\tilde{\rho}$ ,  $\rho_r$  might lead to AR-supply greater than the LWR-supply and therefore no restriction. Summarizing, the augmented supply function (3) always takes values of the LWR-supply or AR-supply, except for the case that the accumulated demand is only slightly bigger than the maximal flux of the outgoing road. In this case, the resulting supply is a linear combination of the AR- and the LWR-supply. Finally, the important issue is whether the augmented model is able to reproduce the capacity drop effect similar to the AR model. Therefore, we analyze the possible cases in which each supply function is larger.

Due to the use of the pressure function (1),  $\tilde{\rho}$  is explicitly given by

$$\tilde{\rho} = p^{-1}(\max\{w(\rho_l) - v(\rho_r), 0\}) = \rho^{\text{max}} \left( \frac{\max\{v(\rho_l) + p(\rho_l) - v(\rho_r), 0\}\gamma}{v^{\text{ref}}} \right)^{\frac{1}{\gamma}}, \quad (7)$$

and the value of  $\tilde{\rho}$  in comparison to  $\rho_l$  can be deduced from the monotonicity of the pressure function, see Table 1.

Table 1: Relation between  $\tilde{\rho}$  and  $\rho_l$

	Value of $\tilde{\rho}$
$\rho_l < \rho_r$	$\tilde{\rho} > \rho_l$
$\rho_l > \rho_r$	$\tilde{\rho} < \rho_l$
$\rho_l = \rho_r$	$\tilde{\rho} = \rho_l$

Two cases for the supply function are further distinguished:

**Case 1** The LWR-supply for  $\rho_r$  exceeds the maximum of the AR-supply, which is exemplarily depicted in Figure 6. This is only possible for  $w_l \leq w_{\text{lim}}$ . In this case, the considered supply is the supply value from the AR model. This result is independent of the value  $\tilde{\rho}$ :

$$S_r^{\text{LWR}}(\rho_r) > S_r^{\text{AR}}(\sigma_l, w_l) \Rightarrow \min\{S_r^{\text{LWR}}(\rho_r), S_r^{\text{AR}}(\tilde{\rho}, w_l)\} = S_r^{\text{AR}}(\tilde{\rho}, w_l).$$

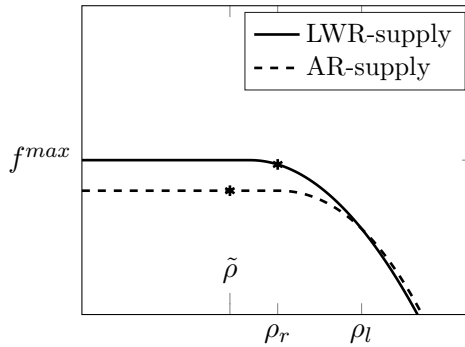


Figure 6: Case 1.

**Case 2** The LWR-supply for  $\rho_r$  exceeds the AR-supply for some values, but it is below the maximum of the AR-supply,

$$S_r^{\text{LWR}}(\rho_r) \leq S_r^{\text{AR}}(\sigma_l, w_l). \quad (8)$$

In this case, the LWR-supply  $S_r^{\text{LWR}}(\rho_r)$  as well as the AR-supply  $S_r^{\text{AR}}(\tilde{\rho}, w_l)$  can be smaller and the value  $\tilde{\rho}$  is significant. We introduce

$$\hat{\rho}(\rho_r) = \operatorname{argmin}_{\rho \geq 0} |S_r^{\text{LWR}}(\rho_r) - S_r^{\text{AR}}(\rho, w_l)|$$

to distinguish two different situations that might occur. Here,  $S_r^{\text{LWR}}(\rho_r) = S_r^{\text{AR}}(\rho, w_l)$  can be achieved and  $\hat{\rho}$  is uniquely determined. This implies solving for the roots of a polynomial with degree  $\gamma + 1$ . Using  $\hat{\rho}$ , we distinguish in the following whether the LWR- or the AR-supply is smaller and therefore, which supply function is used in the ALWR model.

(a) If  $0 \leq \tilde{\rho} \leq \hat{\rho}$ , the AR-supply evaluated at  $\tilde{\rho}$  exceeds the LWR-supply at  $\rho_r$ , see Figure 7. Therefore, we have

$$\min\{S_r^{\text{LWR}}(\rho_r), S_r^{\text{AR}}(\tilde{\rho}, w_l)\} = S_r^{\text{LWR}}(\rho_r)$$

and the ALWR model uses the same supply function as the LWR model in this case.

(b) If  $\hat{\rho} < \tilde{\rho}$ , the ALWR model uses the supply function of the AR model, since in that case  $S_r^{\text{AR}}(\tilde{\rho}, w_l) < S_r^{\text{LWR}}(\rho_r)$ , see Figure 8. Note that in Figure 8  $\hat{\rho}$  is only slightly below  $\tilde{\rho}$ .

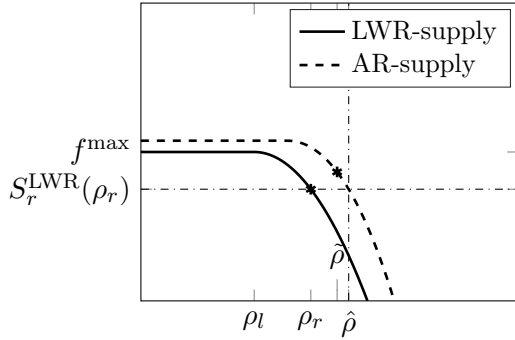


Figure 7: Case 2(a).

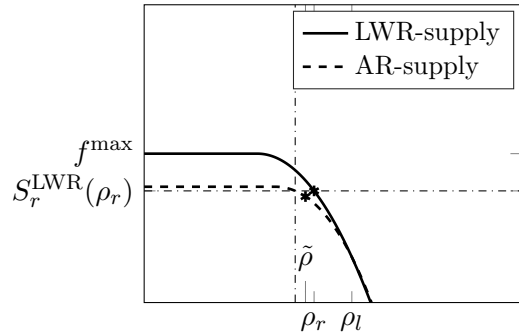


Figure 8: Case 2(b).

### 3.2 Riemann problems for the ALWR model

Based on the discussion of the augmented supply function, we now analyze Riemann problems in the ALWR model. Therefore, we have to investigate whether the AR-supply or the LWR-supply is lower for different combinations of initial states  $\rho_l$  and  $\rho_r$ . Here, we focus on the case  $\gamma = 2$  and  $v^{\text{ref}} = v^{\text{max}}$ . The assumption  $\gamma = 2$  is used to explicitly solve arising equations of degree  $\gamma$ , while the assumption  $v^{\text{ref}} = v^{\text{max}}$  is used to simplify calculations that include  $w_l$ . Note that all considerations can be done analogously for  $\gamma > 1$ . Let us start with some general considerations. We denote by

$$v_l := v(\rho_l) = v^{\text{max}} \left(1 - \frac{\rho_l}{\rho^{\text{max}}}\right),$$

$$w_l := w(\rho_l) = v_l + p(\rho_l) = v^{\text{max}} \left(1 - \frac{\rho_l}{\rho^{\text{max}}}\right) + \frac{v^{\text{max}}}{2} \left(\frac{\rho_l}{\rho^{\text{max}}}\right)^2,$$

$$\begin{aligned}\sigma_l &:= \sigma(\rho_l) = \rho^{\max} \left( \frac{2w_l}{3v^{\max}} \right)^{\frac{1}{2}} = \rho^{\max} \sqrt{\frac{1}{3} \left( \frac{\rho^{\max} - \rho_l}{\rho^{\max}} \right)^2 + \frac{1}{3}}, \\ S^{\text{AR}}(\sigma_l) &:= S^{\text{AR}}(\sigma_l, w_l).\end{aligned}\tag{9}$$

Table 2: Classification of Riemann Problems (for  $\gamma = 2$  and  $v^{\text{ref}} = v^{\max}$ )

			supply	case	
$f_{\text{sum}} > (1 + \epsilon)f^{\max}$	$w_l < w_{\text{lim}}$	$\rho_r \leq \frac{\rho^{\max}}{2}$	AR	I	
		$\rho_r < \sigma_l$	$S^{\text{AR}}(\sigma_l) \geq S^{\text{LWR}}(\rho_r)$	LWR	II
			$S^{\text{AR}}(\sigma_l) < S^{\text{LWR}}(\rho_r)$	AR	III
		$\rho_r > \frac{\rho^{\max}}{2}$	$\rho_l \leq \rho_r$	LWR	IV
			$\rho_r \geq \sigma_l$	$S^{\text{AR}}(\sigma_l) \geq S^{\text{LWR}}(\rho_r)$	AR
		$\rho_l > \rho_r$		$S^{\text{AR}}(\sigma_l) < S^{\text{LWR}}(\rho_r)$	AR
		$w_l \geq w_{\text{lim}}$			LWR

In the following, we show that the models given in Table 2 are the appropriate choices for each of the described situations. Note that for  $\gamma = 2$  and  $v^{\text{ref}} = v^{\max}$ , it is possible to directly compute the density corresponding to a given  $w$ -value:

$$\frac{\rho}{\rho^{\max}} = 1 - \sqrt{2 \frac{w}{v^{\max}} - 1}.\tag{10}$$

Then, for  $\gamma = 2$  and  $v^{\max} = v^{\text{ref}}$ , the limiting case according to (6) and the associated density  $\rho_{\text{lim}}$  are given by

$$w_{\text{lim}} = \frac{3}{2} v^{\max} \left( \frac{1}{4} \right)^{\frac{2}{3}}, \quad \frac{\rho_{\text{lim}}}{\rho^{\max}} = 1 - \sqrt{3 \left( \frac{1}{4} \right)^{\frac{2}{3}} - 1}.$$

The condition  $\rho_r < \sigma_l$  is equivalent to

$$\rho_r < \rho^{\max} \sqrt{\frac{1}{3} \left( \frac{\rho^{\max} - \rho_l}{\rho^{\max}} \right)^2 + \frac{1}{3}}\tag{11}$$

and leads to

$$\frac{\rho_l}{\rho^{\max}} < 1 - \sqrt{1 - 2 + 3 \left( \frac{\rho_r}{\rho^{\max}} \right)^2} = 1 - \sqrt{3 \left( \frac{\rho_r}{\rho^{\max}} \right)^2 - 1}.\tag{12}$$

If the root term is positive and at the same time smaller than one, the value of  $\rho_l$  for which  $\sigma_l = \rho_r$  can be directly computed from (12). This is possible for

$$\frac{\sigma(\rho^{\max})}{\rho^{\max}} = \frac{1}{\sqrt{3}} \leq \frac{\rho_r}{\rho^{\max}} \leq \sqrt{\frac{2}{3}} = \frac{\sigma(0)}{\rho^{\max}}.$$

Hence, the values of  $\rho_r$  for which  $\rho_r < \sigma_l$  holds are generally restricted to

$$\frac{\rho_r}{\rho^{\max}} < \sqrt{\frac{2}{3}}.\tag{13}$$

Next, we analyze condition (8) for  $\rho_r > \frac{\rho^{\max}}{2}$  and  $w_l < w_{\text{lim}}$ . The condition  $S^{\text{AR}}(\sigma_l) \geq S^{\text{LWR}}(\rho_r)$  restricts the values of  $\rho_l$  for a given  $\rho_r$ . Applying

$$S^{\text{AR}}(\sigma_l) = (w(\rho_l) - p(\sigma_l))\sigma_l = \left(\frac{w_l\gamma}{1+\gamma}\right)^{\frac{\gamma+1}{\gamma}} \rho^{\max} \left(\frac{1}{v^{\text{ref}}}\right)^{\frac{1}{\gamma}}$$

on the left-hand side and inserting  $S^{\text{LWR}}(\rho_r) = f(\rho_r)$  on the right-hand side yields

$$\left(\frac{w_l\gamma}{1+\gamma}\right)^{\frac{\gamma}{\gamma+1}} \frac{\rho^{\max}}{v^{\text{ref}}} \geq \rho_r v^{\max} \frac{\rho^{\max} - \rho_r}{\rho^{\max}}$$

and hence

$$w_l \geq \left(v^{\max} \frac{\rho_r}{\rho^{\max}} \frac{\rho^{\max} - \rho_r}{\rho^{\max}} (v^{\text{ref}})^{\frac{1}{\gamma}}\right)^{\frac{\gamma+1}{\gamma}} \frac{\gamma+1}{\gamma}.$$

For  $\gamma = 2$  and  $v^{\text{ref}} = v^{\max}$ , a restriction on  $\rho_l$  can be directly computed by exploiting the relation between  $w$  and  $\rho$  given by (10):

$$\frac{\rho_l}{\rho^{\max}} = 1 - \sqrt{3 \left(\frac{\rho_r}{\rho^{\max}} \frac{\rho^{\max} - \rho_r}{\rho^{\max}}\right)^{\frac{2}{3}} - 1}. \quad (14)$$

If the root term is non-negative,  $\rho_r$  with  $S^{\text{LWR}}(\rho_r) = S^{\text{AR}}(\sigma_l)$  can be directly computed. This is possible for  $\frac{1}{2} < \frac{\rho_r}{\rho^{\max}} \leq \frac{1}{2} + \sqrt{\frac{1}{4} - \left(\frac{1}{3}\right)^{\frac{3}{2}}}$ . Then, the root term in (14) is always smaller than one. Hence,  $S^{\text{AR}}(\sigma_l) > S^{\text{LWR}}(\rho_r)$  is in general possible for  $\frac{1}{2} < \frac{\rho_r}{\rho^{\max}} \leq 1$ . Rearranging (14) for fixed  $\rho_l$  gives a lower bound on  $\rho_r$ :

$$\frac{\rho_r}{\rho^{\max}} \geq \frac{1}{2} + \sqrt{\frac{1}{4} - \left(\frac{1}{3} \left(\frac{\rho^{\max} - \rho_l}{\rho^{\max}}\right)^2 + \frac{1}{3}\right)^{\frac{3}{2}}}. \quad (15)$$

The summarized cases presented in Table 2 lead to a partitioning of the  $\rho_l$ - $\rho_r$ -plane, which is shown in Figure 9. Note that the figure is only valid for  $f_{\text{sum}} > (1 + \epsilon)f^{\max}$ . The AR-supply is applied in the areas I, III, V and VI while the LWR-supply is applied in the areas II, IV and VII.

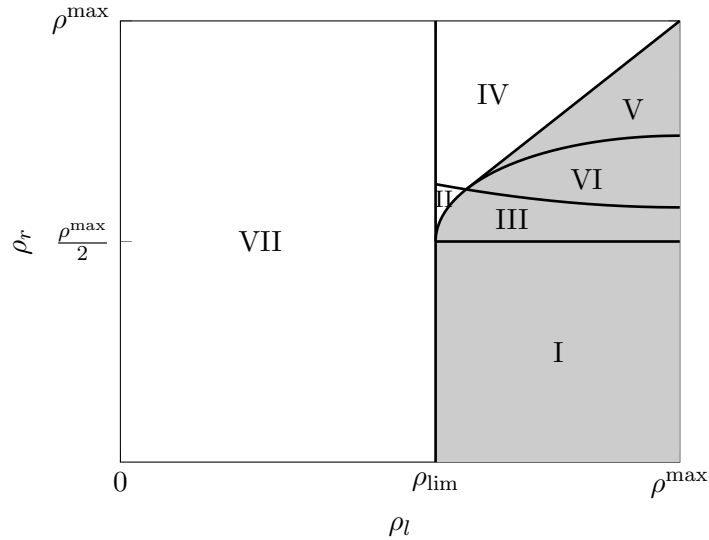


Figure 9: Partitioning of the  $\rho_l$ - $\rho_r$ -plane. Areas for the LWR-supply are in white and areas for the AR-supply are in gray.

Exemplarily, we briefly discuss case VI in Table 2 and the corresponding region in Figure 9. All other cases are explained in the Appendix. Let  $\rho_l > \rho_r$  with  $w_l < w_{\text{lim}}$ ,  $\rho_r > \frac{\rho^{\max}}{2}$ ,  $\rho_r \geq \sigma_l$  and  $S^{\text{AR}}(\sigma_l) < S^{\text{LWR}}(\rho_r)$ . Obviously, since  $S^{\text{AR}}(\sigma_l) < S^{\text{LWR}}(\rho_r)$  is claimed, the AR-supply is applied. Now, since  $\rho_r \geq \sigma_l$ , we get from (9) that

$$\frac{\rho_r}{\rho^{\max}} \geq \sqrt{\frac{1}{3} \left( \frac{\rho^{\max} - \rho_l}{\rho^{\max}} \right)^2 + \frac{1}{3}},$$

which is the lower curve limiting region VI in Figure 9. Next, using the bound computed in (15) but for  $S^{\text{AR}}(\sigma_l) < S^{\text{LWR}}(\rho_r)$ , we get

$$\frac{\rho_r}{\rho^{\max}} < \frac{1}{2} + \sqrt{\frac{1}{4} - \left( \frac{1}{3} \left( \frac{\rho^{\max} - \rho_l}{\rho^{\max}} \right)^2 + \frac{1}{3} \right)^{\frac{3}{2}}},$$

which is the upper limiting curve of region VI in Figure 9.

### 3.3 Theoretical investigations at the junction

In this section, we consider the evolution of the left- and right-hand state  $\rho_l$  and  $\rho_r$  for the Riemann problem at a one-to-one junction with on-ramp within the ALWR model, cf. Figure 2. In comparison to the LWR model and as extension of the analysis in Section 3.2, the most exciting point here is that the evolution of the states at the junction may lead to a change in the “active” model.

We consider roads with infinite lengths and additional to the constant Riemann initial data on the roads, the desired inflow at the on-ramp is set to the maximal flow of the second road. Note that this inflow condition may lead to long queues at the on-ramp that do not further influence the traffic dynamics.

Since the flux function of the LWR model is quadratic, there exist two density values with the same flux value (except for the maximum flux at  $\rho^{\max}/2$ ). To distinguish these density values for a given flux, the following notation is introduced:

$$f_+^{-1}(f(\rho)) = \rho^{\max} \left( \frac{1}{2} + \sqrt{\frac{1}{4} - \frac{f(\rho)}{\rho^{\max} v_{\max}}} \right) \quad f_-^{-1}(f(\rho)) = \rho^{\max} \left( \frac{1}{2} - \sqrt{\frac{1}{4} - \frac{f(\rho)}{\rho^{\max} v_{\max}}} \right).$$

#### 3.3.1 Results for the LWR model

Before analyzing the ALWR model, we briefly review the situation within the LWR model. Two cases can be distinguished regarding the outgoing road for the LWR model:

1.  $\rho_r \in [\frac{\rho^{\max}}{2}, \rho^{\max}]$ ,
2.  $\rho_r \in [0, \frac{\rho^{\max}}{2}]$ .

In the first case, the LWR-supply is  $S = f(\rho_r) \leq f^{\max}$ . Due to our assumption on the desired inflow at the on-ramp, we are in the situation that  $f^{\text{sum}} \geq S$ , i.e., the demand of the incoming road and the on-ramp is at least as large as the supply of the outgoing road and therefore an (accumulated) flux of size  $S$  will enter the outgoing road. Due to the coupling condition with priority parameter  $P$ , the flux from the incoming road to the outgoing road will be  $PS$  if the demand is sufficiently large, or  $D_l(\rho_l)$  otherwise. Accordingly, we have flux  $(1-P)S$  from the on-ramp, or  $S - D_l(\rho_l)$  if  $D_l(\rho_l) < PS$ . Hence, the density  $\rho_r$  stays constant over time at the outgoing road. If  $\rho_l \in [0, \frac{\rho^{\max}}{2}]$ , there will be either no wave (if  $PS \geq f(\rho_l)$ ) or a back-travelling shock wave on the incoming road (if  $PS < f(\rho_l)$ ). In contrast, if  $\rho_l \in [\frac{\rho^{\max}}{2}, \rho^{\max}]$  there will be either a back-travelling shock wave ( $PS < f(\rho_l)$ ), no wave ( $PS = f(\rho_l)$ ) or a rarefaction wave ( $PS > f(\rho_l)$ ) with negative speed on the incoming road. An illustration of the initial conditions and the resulting densities and fluxes in the final situation at the junction with  $PS < f(\rho_l)$  is given in Figure 10.

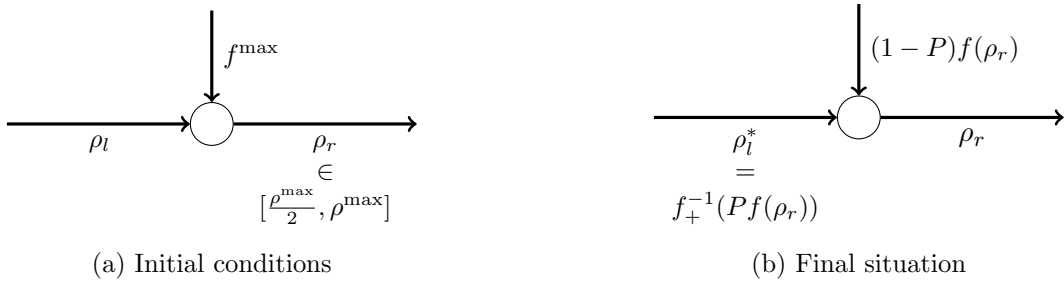


Figure 10: Initial conditions and final situation for  $\rho_r \in [\frac{\rho^{\max}}{2}, \rho^{\max}]$  and  $PS < f(\rho_l)$ .

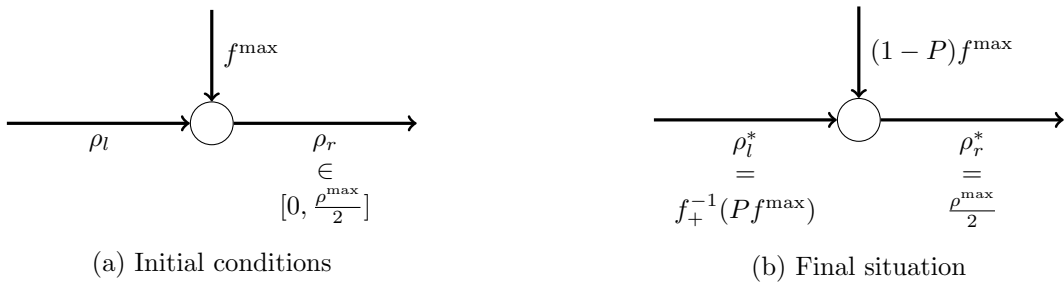


Figure 11: Initial conditions and final situation for  $\rho_r \in [0, \frac{\rho^{\max}}{2}]$  and  $PS < f(\rho_l)$ .

In the second case, the LWR-supply is  $S = f^{\max}$ . On the outgoing road, there will be a rarefaction wave (travelling to the right) and in the limit, the density at the junction on the outgoing road is  $\rho_r^* = \frac{\rho^{\max}}{2}$ . Again, the fluxes are split according to the coupling condition with priority parameter  $P$ . If  $\rho_l \in [0, \frac{\rho^{\max}}{2}]$ , there will be either no wave (if  $PS \geq f(\rho_l)$ ) or a back-travelling shock wave (if  $PS < f(\rho_l)$ ) on the incoming road. If  $\rho_l \in [\frac{\rho^{\max}}{2}, \rho^{\max}]$ , there will be either a back-travelling shock (if  $PS < f(\rho_l)$ ), no wave (if  $PS = f(\rho_l)$ ) or a rarefaction wave with negative speed (if  $PS > f(\rho_l)$ ) on the incoming road. An illustration of the initial conditions and the resulting densities and fluxes in the final situation at the junction with  $PS < f(\rho_l)$  is given in Figure 11.

### 3.3.2 Results for the ALWR model

Now, we turn to the analysis of Riemann problems within a junction in the ALWR model. Due to the construction of the augmented supply function within the ALWR model as minimum of the supply functions of the LWR and the AR model, the solution to the Riemann problem in the ALWR model is restricted by the solution in the LWR model in the sense that the (final) supply of the outgoing road is at most as large as for the same Riemann problem in the LWR model. This means that for  $\rho_r$  in  $[0, \frac{\rho^{\max}}{2}]$ , the arising densities on the outgoing road can never exceed  $\frac{\rho^{\max}}{2}$ . Analogously, for  $\rho_r$  in  $[\frac{\rho^{\max}}{2}, \rho^{\max}]$ , the density on the outgoing road can never exceed  $\rho_r$ . When the current densities at the left-hand and right-hand side of the junction are in a region where the LWR-supply is applied, the solution is identical to the LWR model. But as soon as the combination of the density values is in the region where the AR-supply is applied, the supply drops below the LWR-supply and leads to a different evolution of the solution.

Figure 12 shows the phase space trajectory for a Riemann problem with  $\rho_l \in [0, \rho_{\text{lim}}]$  and  $\rho_r \in [\frac{\rho^{\max}}{2}, \rho^{\max}]$  in the LWR and the ALWR model. Different priority parameters  $P$  are applied at the on-ramp. For the choice of the priority parameter  $P = P_1$ , there is no restriction on the incoming road and the density at the outgoing road remains constant. Therefore, the solution to the Riemann problem is constant in time. Decreasing priority parameters of the first road at some point lead to congestion at the end of the first road (as it is the case for  $P \in \{P_2, P_3, P_4\}$ ). When the phase path

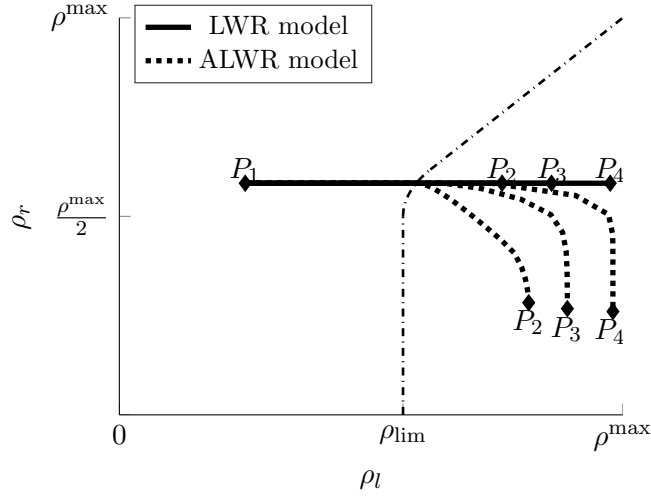


Figure 12: Comparison of the LWR and ALWR model with priority parameters  $P_1 = 0.9$ ,  $P_2 = 0.75$ ,  $P_3 = 0.5$  and  $P_4 = 0.1$  for  $\rho_l \in [0, \rho_{\text{lim}}]$  and  $\rho_r \in [\frac{\rho^{\text{max}}}{2}, \rho^{\text{max}}]$ .

enters the region where the AR-supply is applied, the phase paths of the two models diverge. In the LWR model, only the density at the incoming road increases further. In contrast, in the ALWR model, there is a drop in the density at the outgoing road due to the congestion at the end of the incoming road. This example provides a first evidence that the ALWR model in fact can cover the capacity drop effect and is suitable to consider optimal control problems. The markers at the end of each trajectory indicate the final states that are reached in the respective models for the respective priority parameters.

Figure 13 shows the phase space trajectory for a Riemann problem with  $\rho_r \in [0, \frac{\rho^{\text{max}}}{2}]$ . As described in Section 3.3.1, the density on the outgoing road increases up to  $\frac{\rho^{\text{max}}}{2}$  in the LWR model (since the accumulated demand is high enough here). In the ALWR model we see a different behavior. The density at the outgoing road increases at the beginning, but starts to drop down within the region where the AR-supply is applied.

Figure 14 exemplarily shows some trajectories which move left in the phase plane. Note that for any Riemann problem in the ALWR model, there is at most one change in the supply function applied. There can be either a change from the LWR- to the AR-supply or vice versa. Let

$$\begin{aligned} X_{LWR} &= \{(\rho_l, \rho_r) \in [0, \rho^{\text{max}}]^2 \mid S^{LWR}(\rho_l) \leq S^{AR}(\tilde{\rho}, w_l)\}, \\ X_{AR} &= \{(\rho_l, \rho_r) \in [0, \rho^{\text{max}}]^2 \mid S^{LWR}(\rho_l) > S^{AR}(\tilde{\rho}, w_l)\}. \end{aligned}$$

If the initial densities  $(\rho_l, \rho_r)$  are in  $X_{AR}$ , a change from  $X_{AR}$  to  $X_{LWR}$  in the solution to the Riemann problem will only happen if the density on the incoming road decreases ( $PS > f(\rho_l)$ ). If  $(\rho_l, \rho_r) \in X_{LWR}$ , a change from  $X_{LWR}$  to  $X_{AR}$  will only happen if the density on the incoming road in the LWR model increases and the equilibrium densities  $(\rho_l^*, \rho_r^*)$  of the LWR model are in  $X_{AR}$ . More than one change is not possible and we therefore achieve well-posedness of the ALWR model in the sense of bounded variation of the solutions to Riemann problems.

### 3.3.3 The capacity drop in the solution of the ALWR model

The fluxes in the final situation for the examples considered before are given in Table 3. A capacity drop in the solution for the ALWR model can be seen in all of the cases where the model differs from the LWR model. Note that here, the final fluxes  $f_{\text{ALWR}}^*$  match for  $P_2 - P_4$  since the examples share the same priority parameters as well as the desired inflow from the on-ramp and were constructed such that the final state is located in region I of Figure 9.

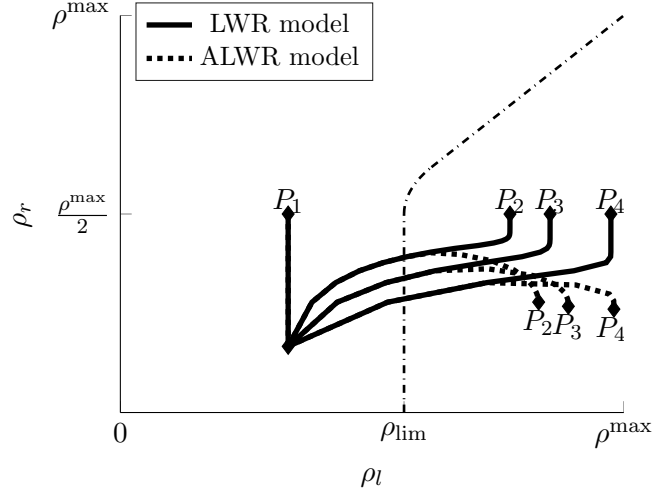


Figure 13: Comparison of the LWR and ALWR model with priority parameters  $P_1 = 0.9$ ,  $P_2 = 0.75$ ,  $P_3 = 0.5$  and  $P_4 = 0.1$  for  $\rho_l \in [0, \rho_{\text{lim}}]$  and  $\rho_r \in [0, \frac{\rho_{\text{max}}}{2}]$ .

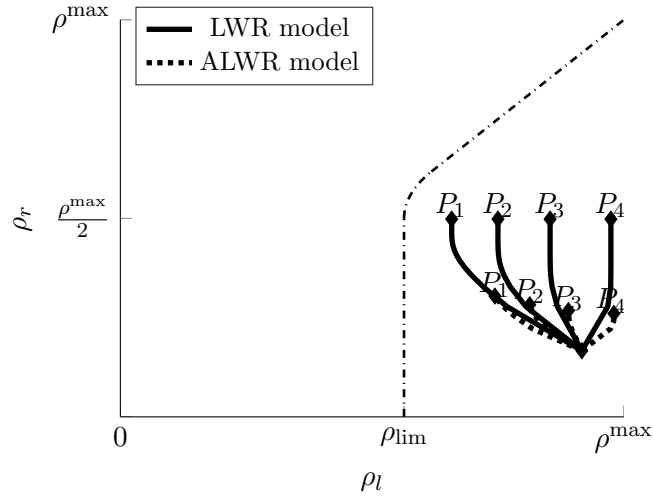


Figure 14: Comparison of the LWR and ALWR model with priority parameters  $P_1 = 0.9$ ,  $P_2 = 0.75$ ,  $P_3 = 0.5$  and  $P_4 = 0.1$  for  $\rho_l \in [\rho_{\text{lim}}, \rho_{\text{max}}]$  and  $\rho_r \in [0, \frac{\rho_{\text{max}}}{2}]$ .

Table 3: Outflow  $f_{\text{ALWR}}^*$  in the final state at the junction with on-ramp (flux values in relation to  $f^{\text{max}}$ )

Priority Parameter	Figure 12		Figure 13		Figure 14	
	LWR	ALWR	LWR	ALWR	LWR	ALWR
$P_1 = 0.90$	0.97	0.97	1	1	1	0.84
$P_2 = 0.75$	0.97	0.81	1	0.81	1	0.81
$P_3 = 0.50$	0.97	0.78	1	0.78	1	0.78
$P_4 = 0.10$	0.97	0.77	1	0.77	1	0.77



## 4 Numerical results for the ALWR model

We consider the on-ramp scenario from [9] with ramp metering as introduced in Section 2.3, see Figure 15 and the parameters given in Table 4. The exponents in the pressure function for the AR model are  $\gamma_i = \gamma = 2$  for all roads and  $\delta = 0.005$  h for the relaxation parameter. The priority parameter  $P$  at the on-ramp equals 0.5 and  $f^{\max} = 2000 \frac{\text{cars}}{\text{h}}$ . At the origin “in” we consider  $f^{\max} = 4000 \frac{\text{cars}}{\text{h}}$ .

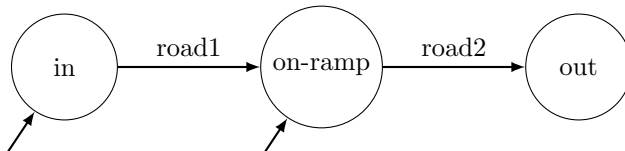


Figure 15: Road network with an on-ramp at the node “on-ramp”.

Table 4: Properties of the roads in Figure 15

road	length [km]	$\rho^{\max} [\frac{\text{cars}}{\text{km}}]$	$v^{\max} = v^{\text{ref}} [\frac{\text{km}}{\text{h}}]$	initial density $[\frac{\text{cars}}{\text{km}}]$
road1	4	180	100	50
road2	2	180	100	50

We consider a time horizon of  $T = 3.0$  hours and the boundary conditions shown in Figure 16.

### 4.1 Discretization of the models

A grid in time and space is introduced for the numerical solution of the different models. The time grid consists of time points  $t^n = n\Delta t$  with  $\Delta t = T/Nt$ , where  $T$  is the time horizon and  $Nt$  the number of time steps. The roads are discretized in space with step size  $\Delta x_e = L_e/Nx_e$ , where  $Nx_e$  denotes the number of intervals on road  $e$ . In the ALWR model, a first order Godunov scheme is used for the computation of the traffic density on the roads - based on the introduced demand and supply functions. Note that coupling and boundary conditions only need to deliver flux values here. For more details, we refer to [8], where the complete description of the Godunov scheme including the proper discretization of coupling and boundary conditions are described for the LWR model. Within the AR model, both density and generalized momentum are computed on each road. As in [9], we apply a splitting approach consisting of a Godunov scheme for the flux term and an implicit Euler scheme for the relaxation term on the right-hand side.

### 4.2 Ramp metering control

For the given scenario, we are interested in minimizing the total travel time

$$\sum_{\text{roads } i} \int_0^T \int_0^{L_i} \rho_i(x, t) dx dt + \sum_{\text{on-ramps } j} \int_0^T l_j(t) dt. \quad (16)$$

To solve this optimization task, we apply a first-discretize-then-optimize approach and adjoint calculus, see also [8,9]. Thus, for given control decisions (time-dependent piecewise constant metering rates), the discretization schemes described in Section 4.1 are always used to evaluate the objective function (16) (using the trapezoidal rule for quadrature). Further, gradient information with respect to the control decisions is computed based on the same discretization, where we refer to [15,17] for more details on the applied software framework. Finally, the SQP solver DONLP2 [22,23] is used for the optimization

of the control decisions. The applied discretization parameters are  $\Delta x = 250$  meters and  $\Delta t = 7.2$  seconds. With the given parameters, a single simulation of the AR model on a notebook with an Intel Core i5-6300U takes roughly half a second - simulations with the ALWR model half of the time.

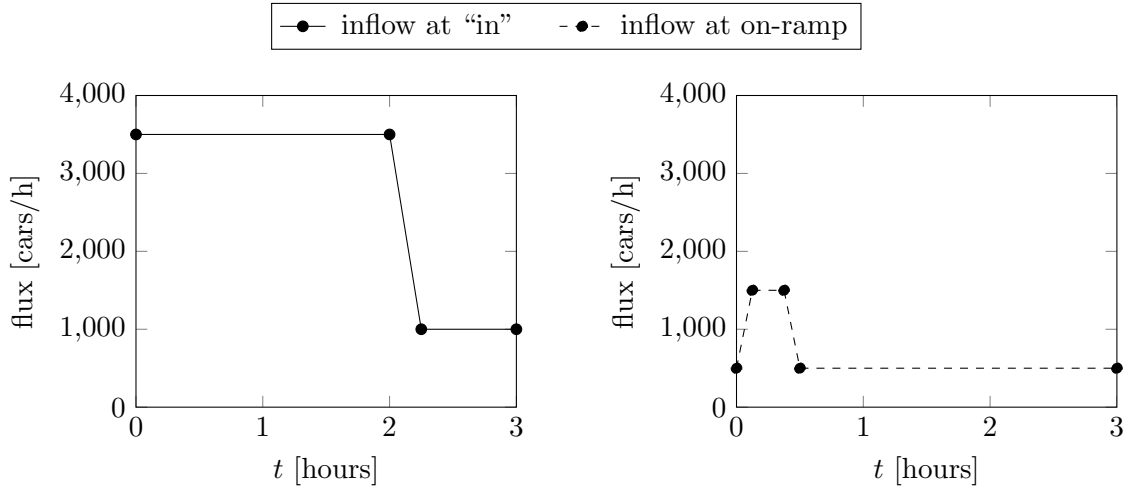


Figure 16: Inflow profiles for the network in Figure 15.

Table 5: Optimization results (total travel time) for the network in Figure 15

	AR	ALWR	LWR
no control	1871.7	2183.1	834.9
optimized ramp metering	795.8	836.2	834.9

Table 5 shows the total travel times for the different models with and without optimization. The resulting queues are shown in Figure 17, where we solely used the AR model for a comparison and to demonstrate the benefit of the optimized control computed with the cheaper ALWR model.

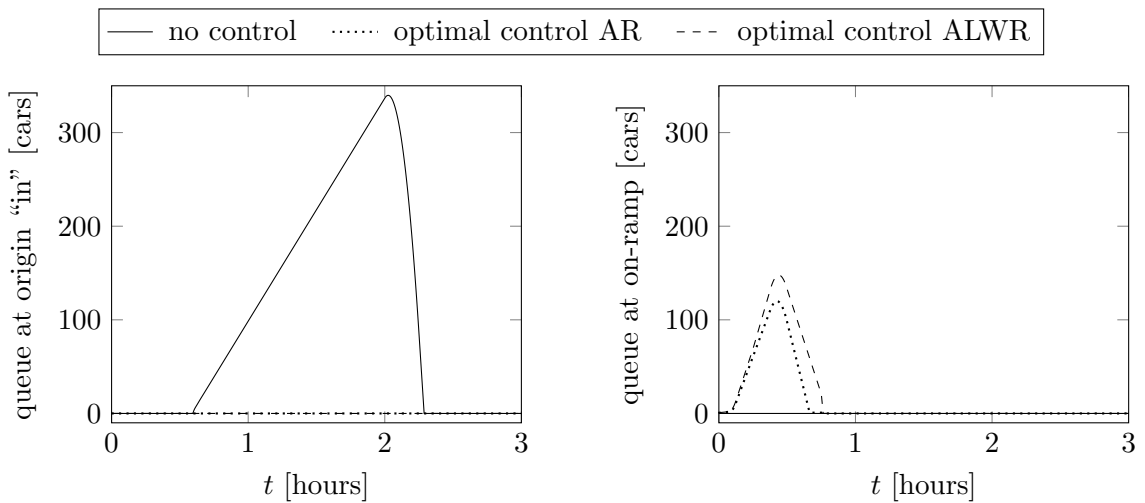


Figure 17: Queue at the origin "in" (left) and the on-ramp (right) with and without optimization.

Running a simulation with the AR model using the optimal control of the ALWR model leads to a total travel time of 809.4, which is less than 2% away from the optimal solution found by optimizing the AR model. Actually, the optimal metering rates for the two models do not differ much, see Figure 18.

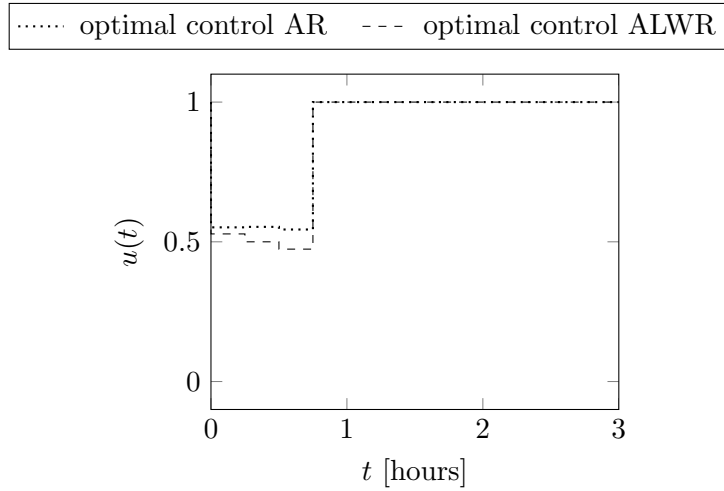


Figure 18: Optimal control of  $u(t)$  at the on-ramp.

Without ramp metering, the queue at the on-ramp stays empty whereas more than 300 cars accumulate in the queue at the origin, see Figure 17. When the optimal control of the AR or the ALWR model is used, the queue at the origin is reduced to zero, while more than 100 cars accumulate in the queue at the on-ramp during the rush-hour time. Figure 19 shows where the improvement in total travel time comes from in the case of ramp metering: The outflow of the system (plot on the right) in the optimized scenarios is clearly above the outflow of the uncontrolled system until it drops to the low inflow level after two hours.

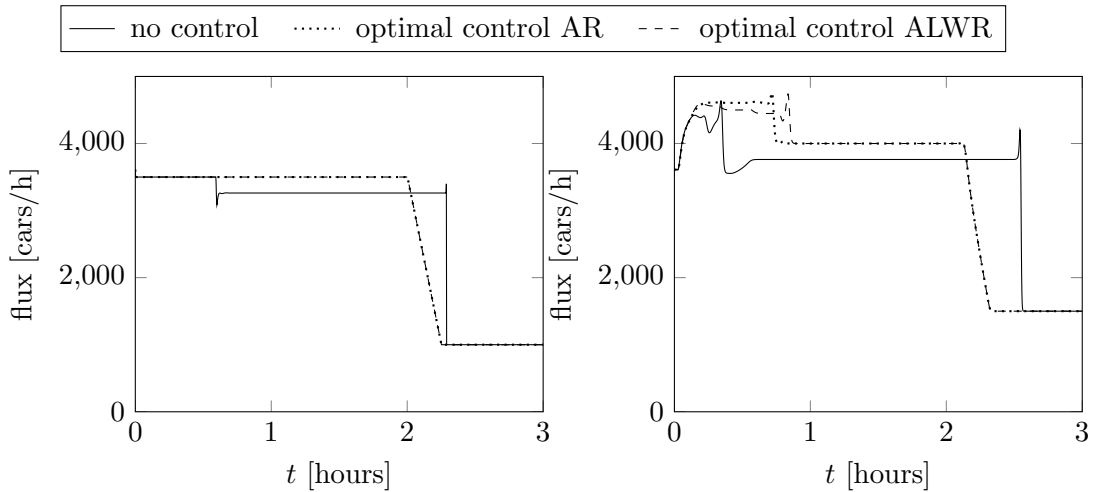


Figure 19: Flow at the origin “in” of the network (left) and at the node “out” (right) with and without optimization.

## 5 Conclusion

We have established a new model for traffic flow which couples the LWR model to boundary conditions of the second order traffic model. The main difference to earlier presented versions of the LWR network model is the shape of the supply function of the outgoing road, which allows for formation of congestion when the incoming road is congested. A discussion of the new supply function was presented and we have shown that the fluxes at the junctions are only dependent on the densities of the adjacent roads. Numerical studies have shown that the ALWR model is able to capture the capacity drop phenomenon and optimization results showed that the ALWR model is a suitable substitute for the second order AR model with relaxation term. Our results show that the ALWR model optimum is extremely close to the optimum of the AR model. At the same time, the computation time was cut to almost half of the computation time of the second order model.

Further research will include the extension of the ALWR coupling conditions to more diverse network structures and a rigorous investigations of Riemann problems.

## Acknowledgment

This work was supported by the DFG grant No. GO 1920/7-1.

## 6 Appendix

**I** The analysis for  $\rho_r \leq \frac{\rho^{\max}}{2}$  and  $w_l \geq w_{\text{lim}}$  is straightforward. The area of admissible combinations of  $\rho_l$  and  $\rho_r$  is shown in area I of Figure 9. By definition, it holds that

$$S^{LWR}(\rho_r) = S^{LWR}\left(\frac{\rho^{\max}}{2}\right) > S^{AR}(\rho) \quad \forall \rho$$

Therefore,  $S^{LWR}(\rho_r) > S^{AR}(\tilde{\rho})$  holds and the AR-supply is applied.

**II** Let  $\rho_l$  and  $\rho_r$  with  $\rho_r > \frac{\rho^{\max}}{2}$ ,  $\rho_r < \sigma(\rho_l)$  and  $S^{AR}(\sigma(\rho_l)) \geq S^{LWR}(\rho_r)$  be given. From (13), (14) and (15) it is known that

$$\begin{aligned} \frac{\rho_r}{\rho^{\max}} &\leq \left(\frac{2}{3}\right)^{\frac{1}{2}} \\ \frac{\rho_l}{\rho^{\max}} &\leq 1 - \sqrt[3]{3 \left( \rho_r \frac{\rho^{\max} - \rho_r}{(\rho^{\max})^2} \right)^{\frac{2}{3}}} - 1 \\ \frac{\rho_r}{\rho^{\max}} &\geq \frac{1}{2} + \sqrt{\frac{1}{4} - \left( \frac{1}{3} \left( \frac{\rho^{\max} - \rho_l}{\rho^{\max}} \right)^2 + \frac{1}{3} \right)^{\frac{3}{2}}}. \end{aligned}$$

Moreover, only values of  $w_l < w_{\text{lim}}$  are considered. Given the restriction (13) and considering only  $\rho_l > \rho_{\text{lim}}$  restricts the values of  $\rho_r$  for which  $\rho_r < \sigma_l$  is possible:

$$\sigma(\rho_{\text{lim}}) = \rho^{\max} \left( \frac{2w_{\text{lim}}}{3v^{\max}} \right)^{\frac{1}{2}} = \rho^{\max} \left( \frac{2}{3v^{\max}} \right)^{\frac{1}{2}} w_{\text{lim}}^{\frac{1}{2}} = \rho^{\max} \left( \frac{1}{4} \right)^{\frac{1}{3}}.$$

Thus, we get the restriction

$$\frac{\rho_r}{\rho^{\max}} < \left( \frac{1}{4} \right)^{\frac{1}{3}} = \frac{\sigma(\rho_{\text{lim}})}{\rho^{\max}}.$$

The area in the  $\rho_l - \rho_r$ -plane which is described by the restrictions above is the area II in Figure 9. For given  $\rho_l$  and  $\rho_r$  in area II, we show that the LWR model is applied. On the one hand, for  $\rho_l \leq \rho_r \Rightarrow \tilde{\rho} = p^{-1}(w_l - v_r) \geq \rho_l$ , we prove that  $\tilde{\rho} \leq \sigma_l$ :

$$p^{-1}(w_l - v_r) \leq \sigma_l \quad \Leftrightarrow \quad \frac{\gamma}{\gamma + 1} w_l \leq v_r$$

Consequently, for  $\gamma = 2$  and  $v^{\max} = v^{\text{ref}}$  it remains to show  $w_l \leq \frac{3}{2}v_r$ . It holds that  $w_l < w_{\text{lim}}$  and  $v_r > v((\frac{1}{4})^{\frac{1}{3}} \rho^{\max})$ . Since  $w_l \leq \frac{3}{2}v_r$  is true for the values of  $\rho_l = \rho_{\text{lim}}$  and  $\rho_r = (\frac{1}{4})^{\frac{1}{3}} \rho^{\max}$ , it holds for all  $\rho_l < \rho_r$  in the considered boundaries. Summarizing, this leads to  $S^{AR}(\tilde{\rho}) = S^{AR}(\sigma_l) > S^{LWR}(\rho_r)$  and the LWR-supply is applied.

On the other hand, for  $\rho_l > \rho_r$ , we know that  $\tilde{\rho} < \rho_l$  and we show that  $\rho_l < \sigma_l$ . For  $\gamma = 2$  and  $v^{\text{ref}} = v^{\max}$ , we get

$$\begin{aligned} \sigma_l - \rho_l &= \rho^{\max} \sqrt{\frac{1}{3} \left( \frac{\rho^{\max} - \rho_l}{\rho^{\max}} \right)^2 + \frac{1}{3}} - \rho_l \stackrel{!}{=} 0 \\ &\Rightarrow \frac{\rho_l}{\rho^{\max}} = -\frac{1}{2} + \sqrt{\frac{5}{4}}. \end{aligned}$$

Since  $\sigma(\rho_l) - \rho_l$  is decreasing in  $\rho_l$ ,  $\sigma(\rho_l) - \rho_l \geq 0 \forall \rho_l \in [0, \rho^{\max}(\frac{1}{2} + \sqrt{\frac{5}{4}})]$ .

Comparing the condition (14) which gives an upper limit for  $\rho_l$  with condition (12), which also gives an upper limit for  $\rho_l$ , shows that the case  $\rho_l > \rho_r$  is only possible for values of  $\rho_r < \rho^{\max}(-\frac{1}{2} + \sqrt{\frac{5}{4}})$  due to the equality of (14) and (12):

$$\begin{aligned} \left( \frac{\rho_r}{\rho^{\max}} \right)^2 &= \left( \frac{\rho_r}{\rho^{\max}} \frac{\rho^{\max} - \rho_r}{\rho^{\max}} \right)^{\frac{2}{3}} \\ &\Rightarrow 0 = \frac{\rho_r}{\rho^{\max}} \left( 1 - \frac{\rho_r}{\rho^{\max}} - \left( \frac{\rho_r}{\rho^{\max}} \right)^2 \right) \end{aligned}$$

which is true for  $\rho_r = 0$  and  $\rho_r = \rho^{\max}(-\frac{1}{2} + \sqrt{\frac{5}{4}})$ . Summarizing, it follows that

$$S^{AR}(\tilde{\rho}) = S^{AR}(\rho_l) = S^{AR}(\sigma_l) > S^{LWR}(\rho_r).$$

**III** Let  $\rho_l$  and  $\rho_r$  be given with  $\rho_r > \frac{\rho^{\max}}{2}$ ,  $\rho_r < \sigma(\rho_l)$ ,  $w_l < w_{\text{lim}}$  and  $S^{AR}(\sigma_l) < S^{LWR}(\rho_r)$ . Since we assume  $S^{AR}(\sigma_l) < S^{LWR}(\rho_r)$ , the AR model is applied. From (11), we know that

$$\frac{\rho_r}{\rho^{\max}} < \sqrt{\frac{1}{3} \left( \frac{\rho^{\max} - \rho_l}{\rho^{\max}} \right)^2 + \frac{1}{3}}$$

Using (8) and (15) for  $S^{AR}(\sigma_l) < S^{LWR}(\rho_r)$ , we get

$$\frac{\rho_r}{\rho^{\max}} < \frac{1}{2} + \sqrt{\frac{1}{4} - \left( \frac{1}{3} \left( \frac{\rho^{\max} - \rho_l}{\rho^{\max}} \right)^2 + \frac{1}{3} \right)^{\frac{3}{2}}}.$$

The area for admissible values of  $\rho_l$  and  $\rho_r$  is marked as III in Figure 9.

**IV** Let  $\rho_l \leq \rho_r$  with  $w_l < w_{\text{lim}}$ ,  $\rho_r > \frac{\rho^{\text{max}}}{2}$  and  $\rho_r \geq \sigma_l$  be given. Since  $\rho_l \leq \rho_r$ , it follows  $\tilde{\rho} = p^{-1}(v(\rho_l) + p(\rho_l) - v(\rho_r))$  and for  $\gamma = 2$  and  $v^{\text{ref}} = v^{\text{max}}$ :

$$\tilde{\rho} \stackrel{(7)}{=} \rho^{\text{max}} \left( 2 \cdot \frac{w_l - v(\rho_r)}{v^{\text{max}}} \right)^{\frac{1}{2}} = \rho^{\text{max}} (v^{\text{max}})^{\frac{1}{2}} \left( \frac{\rho_r - \rho_l}{\rho^{\text{max}}} + \frac{1}{2} \left( \frac{\rho_l}{\rho^{\text{max}}} \right)^2 \right)$$

$$\frac{\partial \tilde{\rho}}{\partial \rho_l} = \rho^{\text{max}} (v^{\text{max}})^{\frac{1}{2}} \left( \frac{-1}{\rho^{\text{max}}} + \frac{\rho_l}{(\rho^{\text{max}})^2} \right) = (v^{\text{max}})^{\frac{1}{2}} \left( \frac{\rho_l}{\rho^{\text{max}}} - 1 \right) < 0. \quad (17)$$

The AR-supply for values above  $\sigma_l$  is

$$S^{AR}(\tilde{\rho}) = (w_l - p(\tilde{\rho}))\tilde{\rho} = (w_l - (w_l - v(\rho_l)))\tilde{\rho} = v(\rho_r)\tilde{\rho}.$$

For increasing  $\rho_l$ ,  $\tilde{\rho}$  decreases and also  $S^{AR}(\tilde{\rho})$ . The highest value of  $\rho_l$  is  $\rho_l = \rho_r$ . Since we assume  $\rho_r \geq \sigma$ ,

$$S^{AR}(\rho_r) = v(\rho_r)\rho_r = S^{LWR}(\rho_r).$$

Thus, for  $\rho_l \leq \rho_r$  it follows that  $S^{AR}(\rho_r) \geq S^{LWR}(\rho_r)$  and the LWR model is applied. The area for admissible values of  $\rho_l$  and  $\rho_r$  is marked in Figure 9 as area IV.

**V** Let  $\rho_l > \rho_r > \sigma(\rho_l)$  be given with  $w_l < w_{\text{lim}}$ ,  $\rho_r > \frac{\rho^{\text{max}}}{2}$  and  $S^{AR}(\sigma_l) \geq S^{LWR}(\rho_r)$ . We show that  $w_l - v_r > 0 \Rightarrow \tilde{\rho} = p^{-1}(w_l - v_r)$  and use information on  $S^{AR}(\tilde{\rho})$  from case IV. Here,  $v_r$  is maximal for

$$\frac{\rho_r}{\rho^{\text{max}}} = -\frac{1}{2} + \sqrt{\frac{5}{4}}$$

and  $w_l$  is minimal for  $\rho_l = \rho^{\text{max}}$  and  $w(\rho^{\text{max}}) = \frac{v^{\text{max}}}{2}$ . The condition  $w_l > v_r$  holds for  $\rho_l = \rho^{\text{max}}$  and therefore holds for all  $\rho_l \leq \rho^{\text{max}}$ . Because  $w_l - v_r > 0$ , we again conclude that  $\frac{\partial \tilde{\rho}}{\partial \rho_l} < 0$  and  $S^{AR}(\tilde{\rho})$  decreases with increasing  $\rho_l$  and the maximum value is for  $\rho_l = \rho_r$ , where  $S^{AR}(\rho_r) = S^{LWR}(\rho_r)$ . It follows that  $S^{AR}(\tilde{\rho}) < S^{LWR}(\rho_r)$  for  $\rho_l > \rho_r$  within the given area, which is area V in Figure 9.

**VII** We analyze more closely the last case, where  $w_l \geq w_{\text{lim}}$ : Since  $w_l \geq w_{\text{lim}}$ , we know that  $\hat{\rho} \geq \rho_r$  (the AR-supply curve is above the LWR-supply curve).

a)  $\rho_l = \rho_r \Rightarrow \tilde{\rho} = \rho_l = \rho_r \leq \hat{\rho}$

b)  $\rho_l > \rho_r \Rightarrow \tilde{\rho} < \rho_l$ , but moreover (for  $\gamma = 2$  and  $v^{\text{ref}} = v^{\text{max}}$ ) it is true that  $\tilde{\rho} \leq \rho_r$ , because one can rewrite  $p^{-1}(w_l - v_r) \leq \rho_r$  for  $\gamma = 2$  and  $v^{\text{ref}} = v^{\text{max}}$  to

$$\rho_l - \rho_r \geq \frac{1}{2\rho^{\text{max}}}(\rho_l - \rho_r)(\rho_r + \rho_l) \quad \Leftrightarrow \quad 2\rho^{\text{max}} \geq \rho_r + \rho_l$$

Which is always true for  $\rho_l, \rho_r \in [0, \rho^{\text{max}}]$ .

c) We consider  $\rho_l < \rho_r$ . We know that  $\tilde{\rho} = p^{-1}(w_l - v_r)$  and from (17) we have that  $\tilde{\rho}$  decreases with  $\rho_l$  and therefore  $S^{AR}(\tilde{\rho})$  decreases for increasing  $\rho_l$ .

Assume  $\rho_l = \rho_r \Rightarrow \tilde{\rho} = \rho_l = \rho_r$ . On the one hand, for  $\rho_r < \sigma_l$ , it follows that  $S^{AR}(\tilde{\rho}) = S^{AR}(\sigma_l)$  and we conclude  $S^{AR}(\tilde{\rho}) = S^{AR}(\sigma_l) > S^{LWR}(\rho_r)$ . On the other hand, for  $\rho_r \geq \sigma_l$ , we conclude  $S^{AR}(\tilde{\rho}) = S^{AR}(\rho_r) = S^{LWR}(\rho_r)$ .

## References

- [1] A. AW AND M. RASCLE, *Resurrection of "Second Order" Models of Traffic Flow*, SIAM Journal on Applied Mathematics, 60 (2000), pp. 916–938.
- [2] A. BRESSAN, S. ČANIĆ, M. GARAVELLO, M. HERTY, AND B. PICCOLI, *Flows on networks: recent results and perspectives*, EMS Surveys in Mathematical Sciences, 1 (2014), pp. 47–111.
- [3] G. M. COCLITE, M. GARAVELLO, AND B. PICCOLI, *Traffic Flow on a Road Network*, SIAM Journal on Mathematical Analysis, 36 (2005), pp. 1862–1886.
- [4] R. M. COLOMBO, *Hyperbolic Phase Transitions in Traffic Flow*, SIAM Journal on Applied Mathematics, 63 (2002), pp. 708–721.
- [5] C. F. DAGANZO, *Requiem for second-order fluid approximations of traffic flow*, Transportation Research Part B, 29 (1995), pp. 277–286.
- [6] M. GARAVELLO AND B. PICCOLI, *Boundary coupling of microscopic and first order macroscopic traffic models*, Nonlinear Differential Equations and Applications, 24 (2017), pp. 24–43.
- [7] P. GOATIN, *The Aw-Rascle vehicular traffic flow model with phase transitions*, Mathematical and Computer Modelling, 44 (2006), pp. 287–303.
- [8] P. GOATIN, S. GÖTTLICH, AND O. KOLB, *Speed limit and ramp meter control for traffic flow networks*, Engineering Optimization, 48 (2016), pp. 1121–1144.
- [9] ———, *Capacity drop and traffic control for a second order traffic model*, Networks and Heterogeneous Media, 12 (2017), pp. 663–681.
- [10] J. M. GREENBERG, *Extensions and Amplifications of a Traffic Model of Aw and Rascle*, SIAM Journal on Applied Mathematics, 62 (2002), pp. 729–745.
- [11] B. HAUT AND G. BASTIN, *A second order model of road junctions in fluid models of traffic networks*, Networks and Heterogeneous Media, 2 (2007), pp. 227–253.
- [12] M. HERTY AND S. MOUTARI, *A macro-kinetic hybrid model for traffic flow on road networks*, Computational Methods in Applied Mathematics, 9 (2009), pp. 238–252.
- [13] M. HERTY, S. MOUTARI, AND M. RASCLE, *Optimization criteria for modelling intersections of vehicular traffic flow*, Networks and Heterogeneous Media, 1 (2006), pp. 275–294.
- [14] M. HERTY AND M. RASCLE, *Coupling Conditions for a Class of Second-Order Models for Traffic Flow*, SIAM Journal on Mathematical Analysis, 38 (2006), pp. 595–616.
- [15] O. KOLB, *Simulation and Optimization of Gas and Water Supply Networks*, PhD thesis, TU Darmstadt, 2011.
- [16] O. KOLB, G. COSTESEQUE, P. GOATIN, AND S. GÖTTLICH, *Pareto-Optimal Coupling Conditions for the Aw-Rascle-Zhang Traffic Flow Model at Junctions*, SIAM Journal on Applied Mathematics, 78 (2018), pp. 1981–2002.
- [17] O. KOLB AND J. LANG, *Simulation and continuous optimization*, in Mathematical optimization of water networks, Birkhäuser/Springer Basel AG, 2012, pp. 17–33.
- [18] M. J. LIGHTHILL AND G. B. WHITHAM, *On Kinematic Waves. II. A Theory of Traffic Flow on Long Crowded Roads*, Proceedings of the Royal Society A: Mathematical, Physical and Engineering Sciences, 229 (1955), pp. 317–345.
- [19] S. MOUTARI AND M. RASCLE, *A Hybrid Lagrangian Model Based on the Aw-Rascle Traffic Flow Model*, SIAM Journal on Applied Mathematics, 68 (2007), pp. 413–436.
- [20] B. PICCOLI AND M. GARAVELLO, *Traffic Flow on Networks*, American Institute of Mathematical Sciences (AIMS), 2006.

- [21] P. I. RICHARDS, *Shock Waves on the Highway*, Operations Research, 4 (1956), pp. 42–51.
- [22] P. SPELLUCCI, *A New Technique for Inconsistent QP Problems in the SQP Method*, Mathematical Methods of Operations Research, 47 (1998), pp. 355–400.
- [23] P. SPELLUCCI, *An SQP method for general nonlinear programs using only equality constrained subproblems*, Mathematical Programming, Series B, 82 (1998), pp. 413–448.